JOURNAL OF MATERIALS SCIENCE 31 (1996) 2071–2080

Fatigue behaviour in a plastic strain-controlled mode of an austenitic stainless steel treated by explosive

M. GERLAND, J. P. DUFOUR*, L. FOUILLAND-PAILLÉ‡, P. VIOLAN, H. N. PRESLES§, J. MENDEZ
Laboratoire de Mécanique et Physique des Matériaux, URA CNRS 863, and § Laboratoire de Combustion et Détonique UPR CNRS 9028, ENSMA, BP 109, 86960 Futuroscope Cedex, France

A surface-treatment technique using primary explosive was applied to a 316L type stainless steel. Some characterizations of the induced mechanical or metallurgical effects are given such as surface roughness, microhardness, residual stresses, microstructure. Fatigue tests were performed in tension–compression in the plastic strain-controlled mode with amplitudes in the range 10^{-3} to 5×10^{-3}. The cyclic behaviour of the treated samples is characterized by a higher cyclic stress amplitude than the untreated material and a shorter fatigue life. The surface damage has been analysed by counting the secondary microcracks after failure. The cyclic behaviour and the damage are discussed taking into account the different induced effects and assuming the treated material to be a composite one, with a highly strengthened surface layer and a quasi-untreated bulk.

1. Introduction

It is well known that fatigue cracks initiate at the surface in homogeneous materials. So, to improve their fatigue resistance, surface treatments that allow them to keep their bulk properties are applied. Among the industrially implemented surface-treatment processes, shot peening is the most frequently used because of its simplicity and the important beneficial results associated with compressive residual stresses. However, the surface roughness of shot-peened materials is generally very high [1–5], introducing detrimental effects on machined specimens. Moreover, when a shot-peened sample is cycled at a high level of stress or strain, the beneficial residual stresses induced by the treatment are quickly deleted [6]. In the last few years, experiments have been undertaken with a new technique using laser-induced shock waves, with good results especially on the induced residual stresses [3, 5, 7]. However, the use of this process on a large scale remains difficult because of both the very limited size of the treated area at each shock and the time between two laser pulses. In addition, there would be difficulties in treating non-planar or complicated shaped samples. More recently, a new technique of surface treatment using shocks has been perfected, based on a primary explosive. The effects induced by this treatment have already been published [8–14]. The aim of this paper is to report the first part of the fatigue behaviour of a 316L type stainless steel treated with this process, when it is cycled in a plastic strain-controlled mode.

2. Experimental procedure

2.1. Material

The studied material was an austenitic stainless steel type AISI 316L (named ICL 167 SPH) whose composition is given in Table I. It was used after heat treating for 1 h at 1050 °C in vacuum (about 5×10^{-4} Pa) and water cooling. The samples (plane samples for metallurgical investigations and cylindrical specimens for fatigue tests, see [8, 9, 14] for shape and dimensions), were first polished before the thermal treatment and polished again before testing to remove the oxide layer up to 1 μm diamond for plane samples and 0.25 μm diamond for fatigue specimens. The mean grain size was about 60 μm.

2.2. Surface-treatment technique

The explosive substance used for surface treatment, based on a primary explosive (lead azide PbN_6), is composed of 95% (wt) PbN_6 and 5% of a mixture of dextrin and nitrocellulose. Because the critical thickness below which the detonation is unable to be propagated is very low ($\simeq$0.1 mm), the explosive substance was applied in a thin layer, like a paint, with a brush on the whole surface to be treated. The

*Present address: Valéo embrayages, Laboratoire de Métallurgie, 5 Av. R. Dumoulin, 80009 Amiens, France.
‡Present address: Laboratoire de Physico-Chimie des Surfaces, ENSAM, BP 3525, 49035 Angers, France.

0022–2461

TABLE I Chemical composition (wt %) of ICL 167 SPH stainless steel

C	Mn	Si	S	P	Ni	Cr	Mo	Cu	B	N_2	Co	As
0.022	1.69	0.31	0.002	0.023	11.90	17.45	2.25	0.110	0.009	0.069	0.190	0.004

detonation was initiated by a laser pulse at the periphery of the area which must be treated, then the detonation spread over the whole area concerned. The explosive layer thickness deposited on the sample was in the range 0.5–1.5 mm. The shock characteristics, pressure and time of pressure application, have been estimated to be close to 3 GPa and 0.6–1.5 μs depending on the explosive thickness (see [13, 14] for details).

2.3. Characterization of the induced effects in the material

The effects induced in the material by the explosive treatment have been investigated by different means: (i) evaluation of the surface topography using a Talysurf profile apparatus; (ii) microhardness measurements with a load of 25 g on sections normal to the treated surface; (iii) microstructure studies by transmission electron microscopy (TEM) on thin foils taken at different depths from the treated surface; (iv) residual stress measurements on the surface and at different depths by X-ray diffraction (see [12, 14] for details on the X-ray diffraction technique).

2.4. Fatigue tests

Fatigue tests have been performed in a symmetrical uniaxial push–pull mode on an electro-mechanical machine at room temperature in air. They were performed in plastic strain-controlled mode with a constant plastic strain rate $\dot{\varepsilon}_p = 2 \times 10^{-3}\ s^{-1}$. The range of the cyclic plastic strain amplitude, $\Delta\varepsilon_p/2$, investigated was from 10^{-3} to 5×10^{-3}. The $\Delta\sigma/2$ stress amplitude necessary to reach the applied plastic strain was continuously recorded up to the sample failure. Tests were conducted on the untreated material and on specimens treated with 1 or 1.5 mm explosive thickness.

3. Results

3.1. Induced effects

The effects induced in the material by treatment have already been reported in detail elsewhere [12–14] and only the main results will be reported here.

3.1.1. Surface roughness

The roughness factor, R_a, given by the arithmetic deviation to a mean line, was close to 0.01 μm before treatment. The evolution of the roughness factor after treatment with explosive thicknesses in the range 0.5–1.5 mm is given in Fig. 1 where it appears that R_a increases with the explosive thickness but remains low, because even for a 1.5 mm explosive thickness, it remains lower than 0.5 μm.

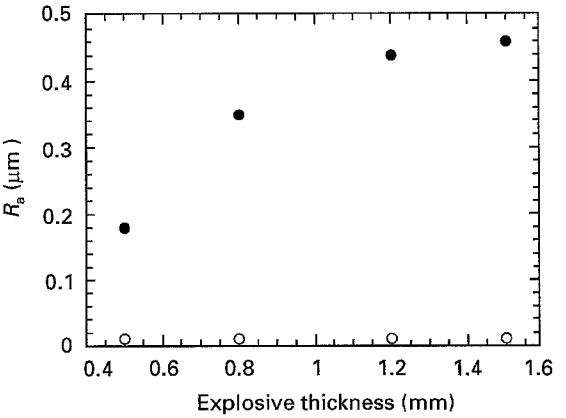

Figure 1 Evolution of the roughness factor, R_a, after treatment, as a function of the explosive thickness: (●) after treatment, (○) untreated.

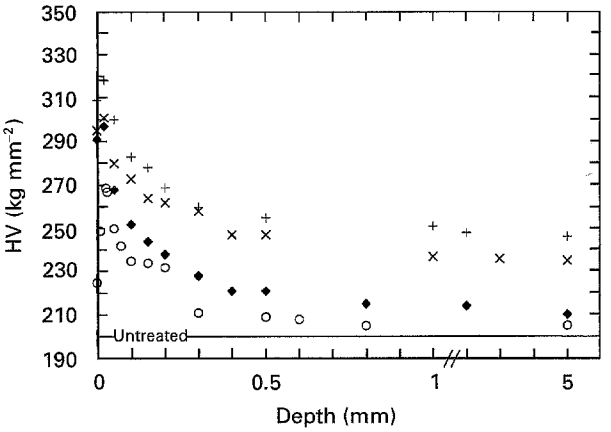

Figure 2 Microhardness profiles on plane samples after treatment, for different explosive thicknesses: (○) 0.5 mm, (◆) 0.8 mm, (×) 1.2 mm, (+) 1.5 mm.

3.1.2. Microhardness

The microhardness profiles of the samples treated with explosive thicknesses between 0.5 and 1.5 mm are given in Fig. 2 which also indicates the mean microhardness value of the untreated material (200 HV). The profiles of the treated materials are characterized by high microhardness values with a maximum located at about 20 μm in depth. The higher the explosive thickness, the higher was hardness throughout the depth. It can be noted that the strengthening reaches the rear face of the samples (5 mm thick). The fact that the maximum of hardness is located at 20 μm in depth and not at the surface is attributed to a thermal effect due to the high temperature of the detonation gases.

3.1.3. Residual stresses

The residual stresses measured on the sample surface by X-ray diffraction are given in Fig. 3 for the

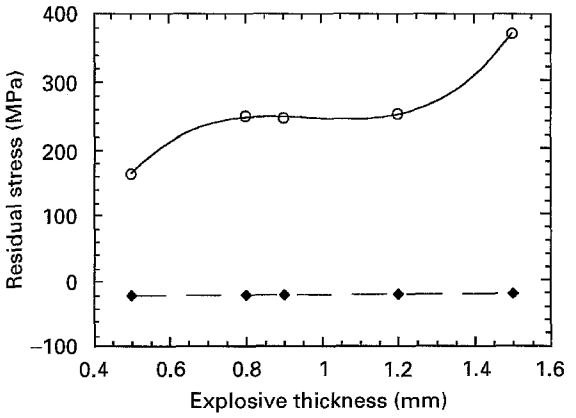

Figure 3 Residual stresses at the surface of the samples after treatment, as a function of the explosive thickness: (○) treated, (◆) untreated.

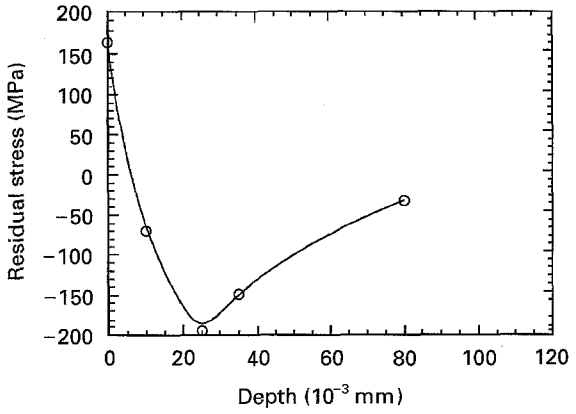

Figure 4 Residual stresses at different depths from the surface, after treatment with an explosive thickness of 0.5 mm.

untreated and polished material and for the different explosive thicknesses. For the reference material, the residual stresses are slightly in compression (− 20 MPa) due to the polishing. On the other hand, after treatment, the stresses are in tension with increasing values in the range 160–370 MPa when the explosive thickness increases. Fig. 4 gives the values of the residual stresses obtained at different depths beneath the surface treated with a 0.5 mm explosive. While at the surface, the residual stresses are in tension (about + 160 MPa), below 10 μm in depth the stresses become compressive and reach values of about − 200 MPa at 25 μm depth, then they decrease, to become close to zero at 90 μm.

3.1.4. TEM observations

A detailed analysis of the microstructure observed by TEM after treatment will be published elsewhere [15] and therefore only the main points will be summarized below: in all cases, the microstructure is characterized by a profuse twinning with maximum density at 20 μm depth (Fig. 5) and which follows the microhardness profiles. Beneath 200 μm depth, the twins become rather rare and are replaced by dislocations distributed in the form of dense walls generally along three slip directions in each grain. The dislocation density

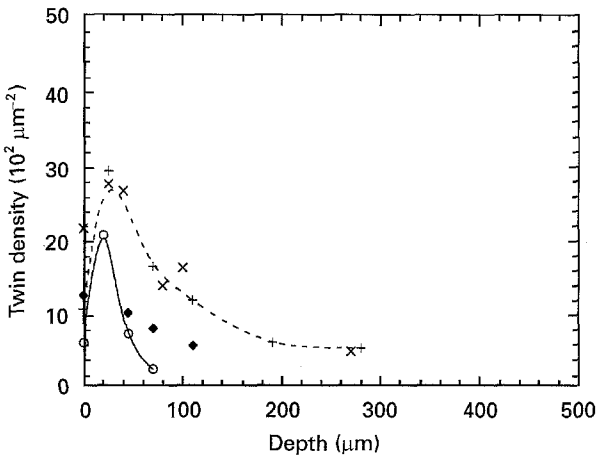

Figure 5 Twin density evolution versus depth for different explosive thicknesses: (○) 0.5 mm, (◆) 0.8 mm, (×) 1.2 mm, (+) 1.5 mm.

progressively decreases when depth increases. Moreover, for the highest explosive thickness (1.5 mm), at the surface, a very thin layer (less than 1 μm thick) of recrystallized grains with a mean diameter of about 30 μm is observed before the beginning of the twins.

3.2. Fatigue results

3.2.1. Cyclic behaviour

The evolution of the stress amplitude, $\Delta\sigma/2$, as a function of the number of cycles in semi-logarithmic diagrams are given for both treated and untreated materials in Figs 6–8 for the plastic strain amplitudes $\Delta\varepsilon_p/2 = \pm 10^{-3}$, $\pm 2\times10^{-3}$ and $\pm 5\times10^{-3}$, respectively, and for an explosive thickness of 1 mm. For the amplitude of 10^{-3}, a test with a specimen treated with an explosive thickness of 1.5 mm is added (Fig. 6). For every plastic strain amplitude, the treated material exhibits an increase in the mechanical properties compared to the reference state, in that the stress amplitude at the first cycle is about 40–60 MPa higher in the treated state; this behaviour persists during the near totality of the fatigue life except for the amplitude of 5×10^{-3}. However, for each amplitude, the fatigue life of the treated material is shorter than the reference one (Table II). The cyclic behaviour of

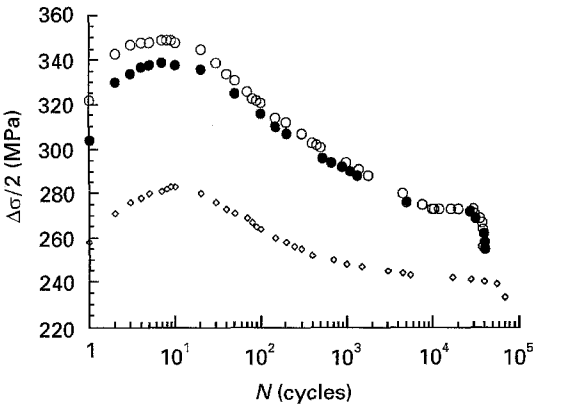

Figure 6 Cyclic behaviour of ICL 167 SPH stainless steel at a constant plastic strain amplitude $\Delta\varepsilon_p/2 = 10^{-3}$ for three different states: (◇) untreated material, and specimens treated with an explosive thickness of (●) 1 and (○) 1.5 mm.

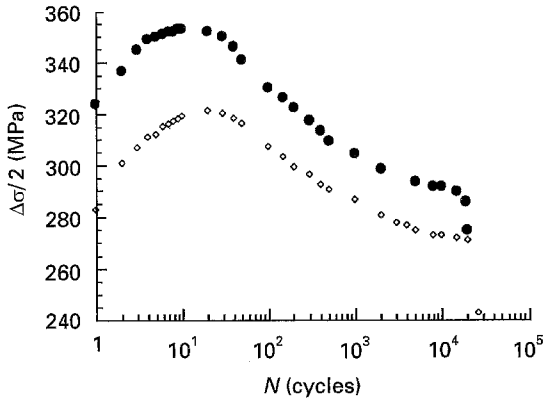

Figure 7 Cyclic behaviour of ICL 167 SPH stainless steel at a constant plastic strain amplitude $\Delta\varepsilon_p/2 = 2 \times 10^{-3}$ for the (◇) untreated material and (●) a specimen treated with an explosive thickness of 1 mm.

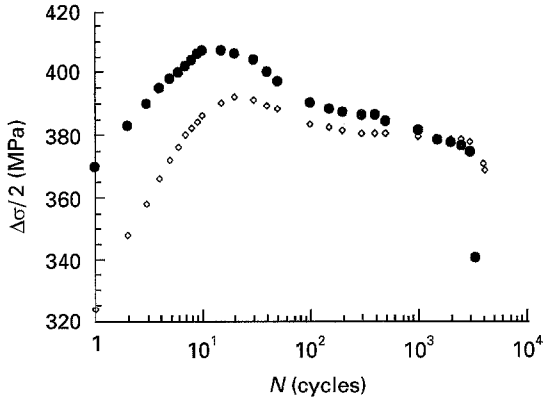

Figure 8 Cyclic behaviour of ICL 167 SPH stainless steel at a constant plastic strain amplitude $\Delta\varepsilon_p/2 = 5 \times 10^{-3}$ for the (◇) untreated material and (●) a specimen treated with an explosive thickness of 1 mm.

TABLE II Fatigue lives of ICL 167 SPH stainless steel for the reference and treated states

Plastic strain amplitude	Fatigue life	
	Untreated material	Treated material
10^{-3}	72000	41360 with 1 mm 39400 with 1.5 mm
2×10^{-3}	26175	19750
5×10^{-3}	4200	3300

the reference state at every strain amplitude is characterized by a primary stage during 10–20 cycles, followed by a softening stage up to 5000 cycles for the lowest strain amplitude and about 200 cycles for the highest one. The stress level is rather stabilized during the main part of the test, up to the fast decrease of stress corresponding to the propagation of a macrocrack leading to failure. In the treated material, the primary hardening stage is shorter than in the reference state, but on the other hand, the softening stage occupies about 90% of the fatigue life, so that the stabilized stage is quite non-existent. The difference of 40–60 MPa between the curves of the treated and the reference materials at the first cycle slowly decreases to 30 MPa (or 20 MPa) for the lowest strain amplitude (or for $\Delta\varepsilon_p/2 = 2 \times 10^{-3}$), but decreases more quickly for the highest strain amplitude; in the latter case, the difference becomes zero at half the fatigue life, then it is inverted. Except for this last case, the cyclic stress increase induced by the treatment is rather stable. The Manson–Coffin curves ($\Delta\varepsilon_p/2 - N_f$, where N_f is the number of cycles to failure) are drawn in Fig. 9 where it clearly appears that the fatigue life of the treated materials is shorter than that of the reference material over the entire strain amplitude range studied. However, it can be noticed that the treated material is subjected to an elastic strain amplitude (thus a total strain amplitude) higher than the untreated one. If the two materials are compared with the same stress amplitude, such as in Fig. 10, where $\Delta\sigma(N_f/2)$ corresponds to the stress amplitude at half the fatigue life, the treated material behaves better than the untreated one; furthermore, the lower the plastic strain amplitude, better is the behaviour of the treated material in comparison with the reference one.

In order to understand the effect of the treatment on the cyclic behaviour of the two states, treated and untreated materials, a study of the surface damage was performed.

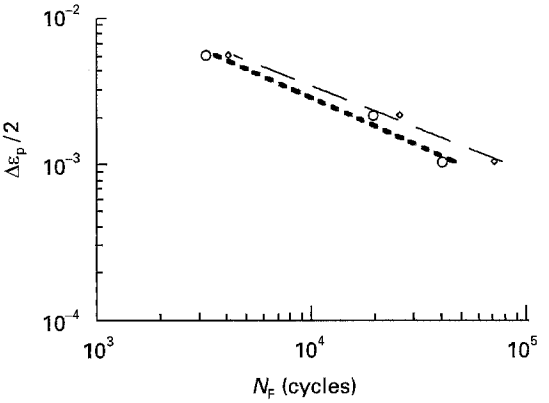

Figure 9 Manson–Coffin curves of ICL 167 SPH stainless steel for the (○) treated and (◇) untreated materials.

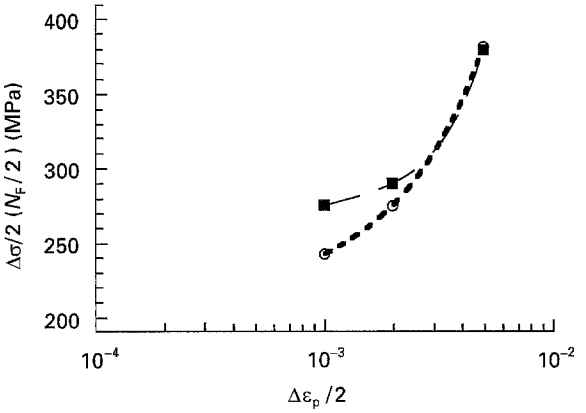

Figure 10 Cyclic stresses $\Delta\sigma/2$ at half the fatigue life as a function of the plastic strain amplitude $\Delta\varepsilon_p/2$ of ICL 167 SPH stainless steel for the (■) treated and (○) untreated materials.

3.2.2. Surface damage

The examination of the sample gauge length by scanning electron microscopy (SEM) after cycling to failure allows the modes of deformation and cracking, both on reference and treated specimens, to be emphasized.

The surface of the reference material is characterized by a high density of intense slip bands generally straight and with sizeable extrusions. For the lowest strain amplitude, the deformation is very heterogeneous from one grain to another one. When the strain amplitude increases, both the number of grains with slip bands and the density of these bands increase. Microcrack initiation is located in the intense slip bands, then the microcracks propagate from one grain to another by changing slip-band systems, so that the microcrack remains macroscopically normal to the stress axis. The propagation is thus mainly transgranular [16].

The surface of the explosive-treated material is characterized by a cracking with very few slip bands, especially for the lowest strain amplitude, even in the near proximity of the main crack (Fig. 11). However, some slip bands can be hidden by the adherent residues of the detonation products which appear locally in Fig. 11. In spite of the few visible slip bands, the microcrack initiation is mainly transgranular. For the higher strain amplitudes, the microcrack initiation is still predominantly transgranular, but the cracking exhibits a more ramified aspect (Fig. 12), especially for $\Delta\varepsilon_p/2 = 5 \times 10^{-3}$ where some grains are saturated with microcracks (Fig. 13).

A quantitative analysis of the surface damage consisted in counting the secondary microcracks on the gauge length after the fatigue test was performed on every sample. Moreover, every microcrack was measured and classified according to its length, by classes of 30 μm (half of the mean grain size). All these data enable the total density of secondary microcracks (indicated in microcracks per square millimetre) to be calculated and histograms of the microcrack density in each length class to be drawn. Table III gives the total secondary microcrack densities as a function of the plastic strain amplitude for the two states of the material, and Fig. 14 shows the evolution of these

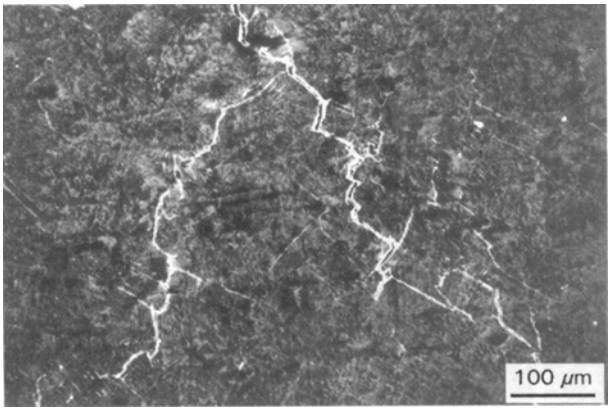

Figure 11 Scanning electron micrograph showing the main crack and secondary microcracks without slip bands in the treated material (1 mm explosive thickness), after cycling at $\Delta\varepsilon_p/2 = 10^{-3}$.

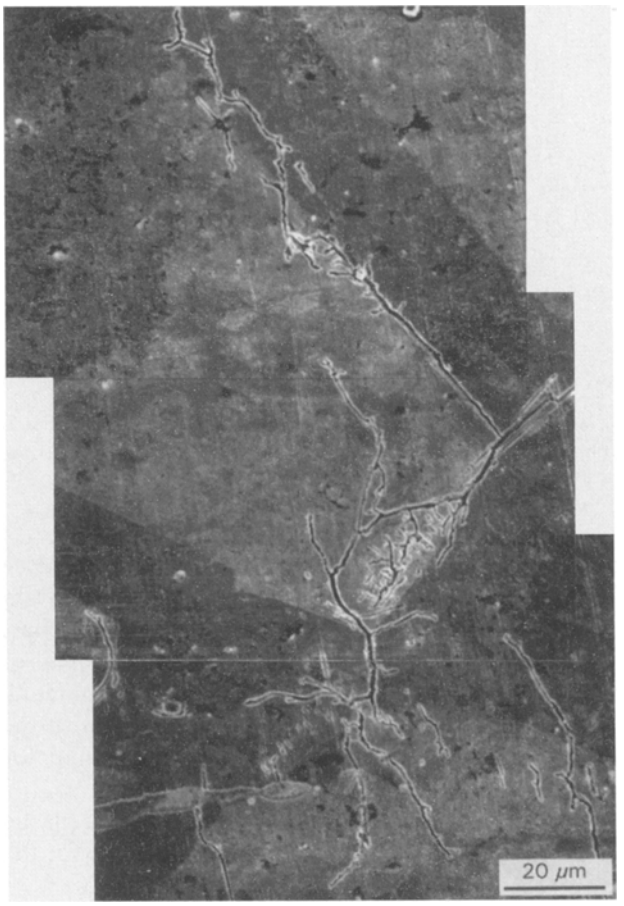

Figure 12 Scanning electron micrograph showing microcracks with a ramified aspect in the treated material after cycling at $\Delta\varepsilon_p/2 = 2 \times 10^{-3}$.

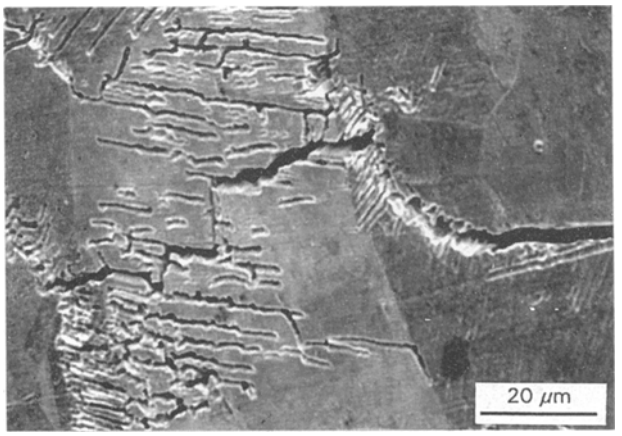

Figure 13 Scanning electron micrograph showing the main crack and a grain saturated with short microcracks in the treated material after cycling at $\Delta\varepsilon_p/2 = 5 \times 10^{-3}$.

TABLE III Total secondary microcrack density as a function of the plastic strain amplitude for the two states of the material

	Total density (microcracks/mm^2)	
$\Delta\varepsilon_p/2$	Reference state	Treated state
10^{-3}	12	27 (1 mm explosive thickness) 62 (1.5 mm explosive thickness)
2×10^{-3}	23	67 (1 mm)
5×10^{-3}	29	160 (1 mm)

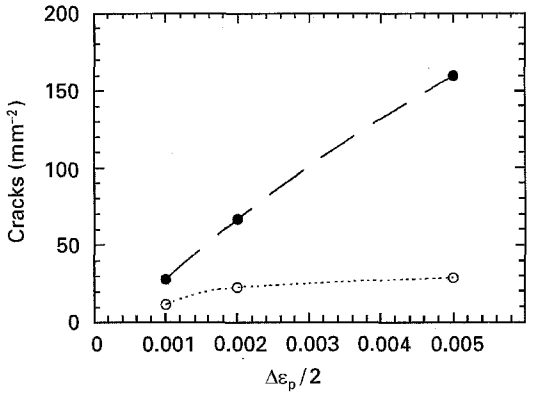

Figure 14 Evolution of the total secondary microcrack densities in the two states of ICL 167 SPH stainless steel as a function of the plastic strain amplitude: (○) untreated, (●) treated.

densities with the strain amplitude. For the reference state, the microcrack density increases with the strain amplitude but seems to be saturated for the highest strain level with a density value of about 30 microcracks/mm^2. On the contrary, for the treated material, the microcrack density drastically increases with the strain amplitude, to reach 160 microcracks/mm^2 for $\Delta\varepsilon_p/2 = 5 \times 10^{-3}$.

The histograms corresponding to the three plastic strain amplitudes are shown in Figs 15 and 16 for the

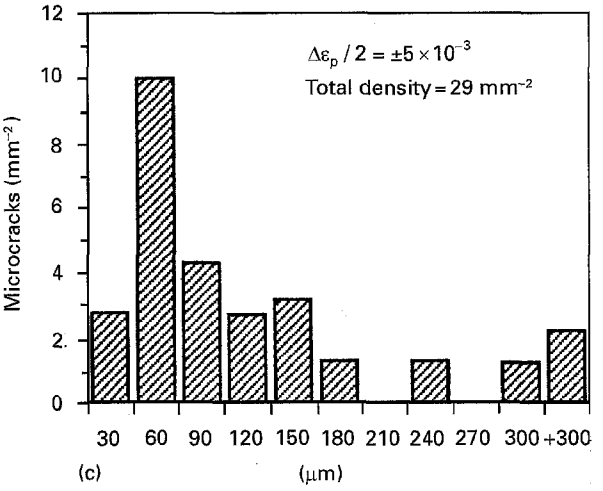

Figure 15 Continued.

untreated and treated states, respectively. The reference state is characterized by the usual distribution with a maximum density in the second section [17, 18] and a low density of short microcracks (length < 30 μm). On the other hand, in the treated material, the number of microcracks shorter than 30 μm is considerably higher than in the reference state for the three strain amplitudes. The examination of the length classes between 30 and 120 μm shows microcrack

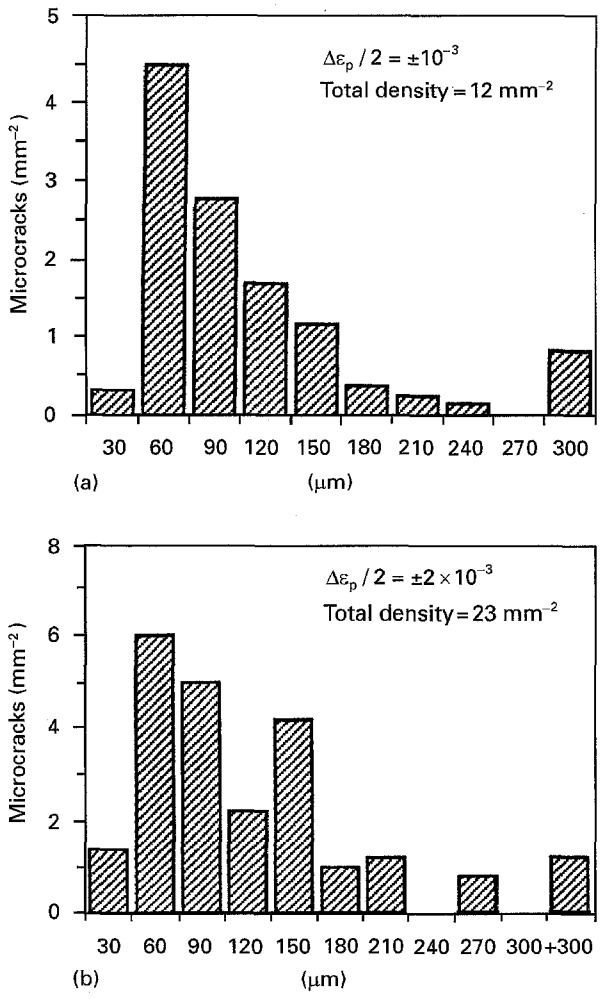

Figure 15 Histograms showing the secondary microcrack distribution in the untreated material for the three plastic strain amplitudes.

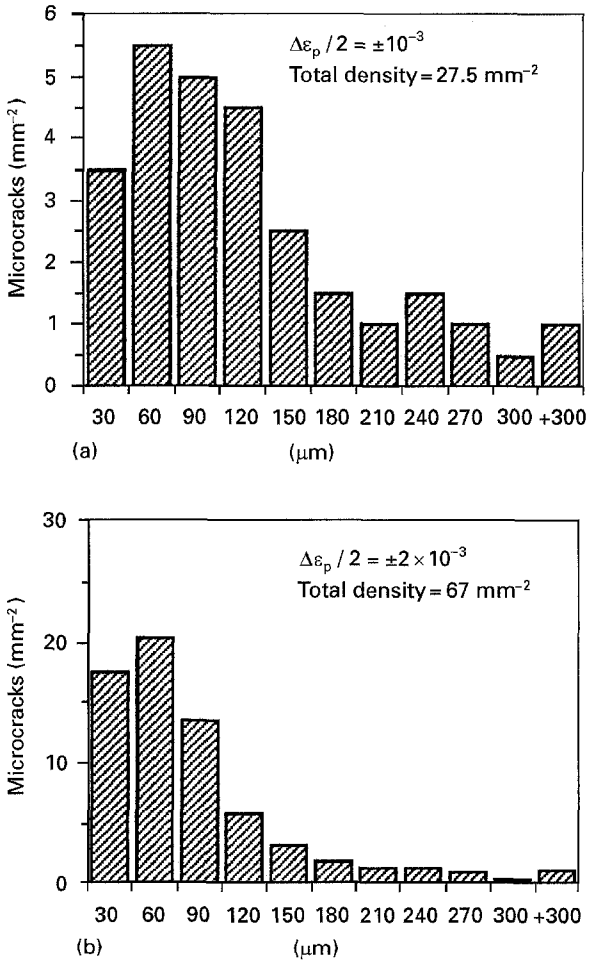

Figure 16 Histograms showing the secondary microcrack distribution in the treated material for the three plastic strain amplitudes.

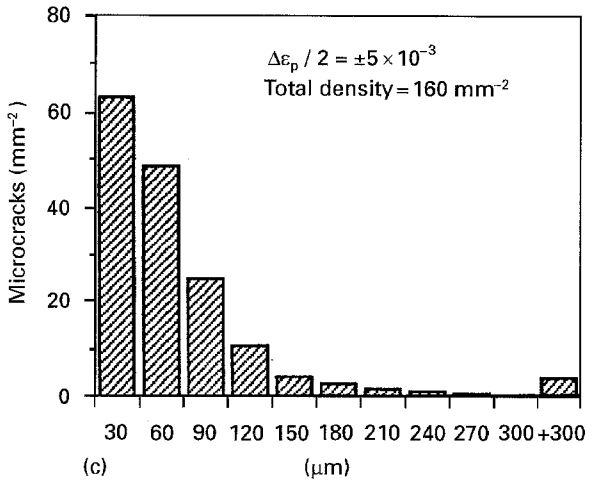

Figure 16 Continued.

densities higher in the treated material than in the reference one, especially for the highest strain amplitude. Beyond 120 μm, the densities of microcracks are rather similar except for the lowest strain amplitude where they are higher in the treated material.

3.2.3. Evolution of the microhardness after cycling

Before cycling, the reference microhardness value of the untreated material was 200 HV. After cycling, the fatigue specimens were cut perpendicular to the stress axis at a distance of 2 mm from the main crack and microhardness measurements were performed from the outer surface to the centre of the samples with a 25 g load. After cycling, for the untreated material, an increase of the microhardness was noted due to cyclic strengthening. The corresponding mean microhardness values, constant along the profile, were 225 HV for $\Delta\varepsilon_p/2 = 10^{-3}$, 240 HV for $\Delta\varepsilon_p/2 = 2 \times 10^{-3}$, and 290 HV for $\Delta\varepsilon_p/2 = 5 \times 10^{-3}$.

The microhardness profiles obtained on a treated specimen cycled at the three plastic strain amplitudes are given in Fig. 17. For $\Delta\varepsilon_p/2 = 10^{-3}$, the aspect of the microhardness profile is not very different from the uncycled and treated material profile. However, its maximum is less high than in the uncycled material. For $\Delta\varepsilon_p/2 = 2 \times 10^{-3}$, the maximum microhardness is not located near the surface but at about 100 μm depth. For $\Delta\varepsilon_p/2 = 5 \times 10^{-3}$, the microhardness profile is completely modified: the microhardness is markedly lower at the surface than at a great depth. The higher the plastic strain amplitude, the higher was the decrease of the microhardness after cycling in the surface layers. This phenomenon can be explained by the extent of the surface damage in the treated and cycled material, because at failure, the secondary microcrack density reaches values of 67 or 160 mm^{-2} for $\Delta\varepsilon_p/2 = 2 \times 10^{-3}$ or 5×10^{-3}, respectively. The presence of voids in such a quantity (see Fig. 13) thus leads to an apparent reduction of microhardness. On the other hand, the microhardness profiles of the lowest strain amplitudes are located above the corresponding value of the untreated and cycled material, while for the highest strain amplitude the microhardness profile is located below the corresponding value of the untreated and cycled material. This fact can be related to the cyclic behaviour (see Figs 6–8) where it appears that the treated material exhibits higher cyclic stresses than the untreated material for the lowest strain amplitudes and inversely for the highest strain amplitude. However, the differences between the curves of the treated and uncycled sample, that treated and cycled at 10^{-3}, and that treated and cycled at 2×10^{-3} in the area 100–300 μm, are not significant and can be due to measurement and treatment scattering, because there is probably no hardening induced by cycling in this area, the microhardness of the treated and uncycled sample being already higher than the microhardness of the untreated and cycled samples at the amplitudes of 10^{-3} and 2×10^{-3}.

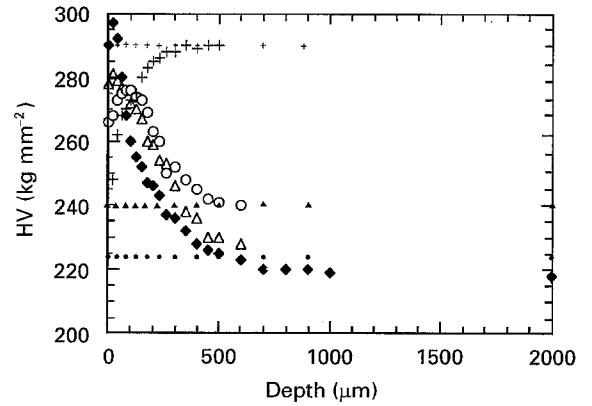

Figure 17 Microhardness profiles on a normal section of (△, ○, +, ◆) treated and (+, ▲, ●) untreated specimens after cycling at a constant plastic strain amplitude $\Delta\varepsilon_p/2$ = (◆) uncycled, (△, ●) 10^{-3}, (○, ▲) 2×10^{-3}; and (+, +) 5×10^{-3}.

4. Discussion

For the three plastic strain amplitudes, the cyclic hardening curves (Figs 6–8) show the effect of the induced strengthening and the stability of this treatment, especially for $\Delta\varepsilon_p/2 = 10^{-3}$ and 2×10^{-3} where it persists up to failure, contrary to what is generally observed after shot peening [6]. The cyclic behaviour is partly explained by the mechanical properties of the highly strengthened layers on about the first 300 μm where, as we have already shown [10], the yield strength is estimated to be close to 850 MPa instead of 250 MPa in the untreated material. In these layers, the microstructure is mainly composed of numerous twins [13, 14]. A detailed analysis of the microstructure will be published elsewhere [15]. Now, in order to understand the behaviour of the treated material during a cycle, we will consider it to be a composite material with a thin hardened outer part and the untreated bulk. So let us consider such a treated specimen cycled with an applied plastic strain amplitude, $\Delta\bar{\varepsilon}_p$; the resulting total strain amplitude, $\Delta\varepsilon_T$, is identical in the bulk as well as in the highly hardened surface layers. However, the plastic strain amplitude in each part, the bulk and the surface layers, is not identical to the applied $\Delta\bar{\varepsilon}_p$, as is schematically illustrated in Fig. 18

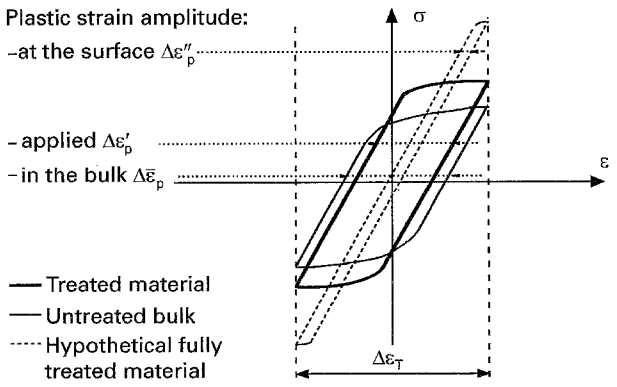

Figure 18 Schematic drawing showing the plastic strain amplitudes of the treated and untreated samples in the bulk and in the highly strengthened surface layers.

and explained below. This figure shows the hysteresis loops (σ–ε) of the untreated material (with a fine and continuous line) and of a hypothetical fully treated material – as in the first 300 μm which then exhibits a high yield strength of about 850 MPa [10].

Now, a specimen treated as in the previous paragraphs and cycled with the same total strain amplitude, $\Delta\varepsilon_T$, described by the vertical lines, which corresponds to the total isodeformation of the two parts of the treated specimen, will show a hysteresis loop similar to that drawn with a thick line. The intersection of the vertical lines with the prolongation of the hysteresis loop of the untreated material, emphasizes the fact that the plastic strain amplitude, $\Delta\varepsilon'_p$, in the bulk of the treated material is increased compared to the applied $\Delta\bar{\varepsilon}_p$. On the contrary, for the same total strain amplitude, the hysteresis loop of the fully treated specimen shows that the plastic strain amplitude, $\Delta\varepsilon''_p$, in the surface layers is markedly lower than the applied $\Delta\bar{\varepsilon}_p$.

Therefore, the fact that the fatigue lives of the treated samples are shorter than that of the untreated specimen when they were tested under plastic strain amplitude could be explained by several factors:

(i) the irregularities of the treated surface, as can be seen with the measurement of the R_a factor (see Fig. 1), favour the initiation of microcracks;

(ii) in the treated material, the residual stresses at the surface are in tension which tends to lower the fatigue life by making microcrack initiation easier;

(iii) the very high cyclic stress of the treated specimens compared to the untreated ones;

(iv) as described in the above paragraph, the plastic strain amplitude in the bulk of the treated sample is higher than that of the untreated specimen and, as a consequence, microcrack propagation which is governed by the plastic strain amplitude [19] is enhanced;

(v) the surface layers of the treated material are composed of numerous twins, and it is known that such a structure makes initiation and propagation of microcracks easier [20].

In order to verify these points, two specimens were treated with a 1.5 mm explosive thickness then polished to remove a layer of 40 μm from the first one and 75 μm from the other one. These removals allow the surface to be subjected to high stresses in compression for the first one, and stresses close to zero for the second one, if it is assumed that the residual stresses in depth after a treatment with 1.5 mm are not very different to those of material treated with 0.5 mm explosive. In Fig. 4, it appears that after a removal of 40 μm, the residual stresses are in compression (about − 150 MPa) while at the surface they are in tension (about + 160 MPa), and at 75 μm in depth, they are very slightly in compression (− 35 MPa). Now it is well known that residual stresses in compression tend to delay the microcrack initiation and to prevent their propagation [2].

The curves giving the evolution of the cyclic stress amplitude of the treated samples are not given, because they are similar to that shown in Fig. 6 for the material treated with an explosive thickness of 1.5 mm. This behaviour is not surprising because of the very low thickness of the removed layers in comparison with the whole treated thickness. The fatigue lives and the values of the cyclic stress at half the fatigue life are given in Table IV.

As mentioned above, the cyclic stress evolution of the polished specimens after treatment is not different from that of the treated one and thus the cyclic stress amplitude at half the fatigue life is identical for the three tests (275 MPa). On the other hand, the fatigue life of the specimen polished of 40 μm is increased. This increase can be related to the compressive residual stresses present at the surface after a removal of 40 μm. The increase of the fatigue life (51 000 cycles as against 39 400 cycles) can also be partly due to the better surface due to the polishing (R_a close to zero as against 0.45 μm). However, the fatigue lives of the treated and the polished material are still shorter than that of the untreated material. This is explained by the fact that at 40 or 75 μm depth, the twin density is high after a treatment with an explosive thickness of 1.5 mm, as shown in Fig. 5, and then initiation and propagation of microcracks are made easier along twin boundaries. This point is confirmed by the analysis of the surface damage as explained in the next paragraph.

The histograms giving the crack distribution at failure on the specimens treated with 1.5 mm explosive thickness then polished before cycling are given in Fig. 19. The total microcrack density is lower on the polished specimens, especially after a polishing of 40 μm. As the histograms are similar beyond a length of 120 μm, the difference in the total density between the three samples comes from the first three classes. In the first class, the microcracks of the two polished

TABLE IV Fatigue lives and cyclic stresses at half the fatigue life of treated samples with or without subsequent polishing

Specimen	Fatigue life	$\Delta\sigma/2(N_F/2)$ (MPa)
Treatment with 1.5 mm	39 400	275
Treatment with 1.5 mm + polishing 40 μm	51 000	275
Treatment with 1.5 mm + polishing 75 μm	39 460	275

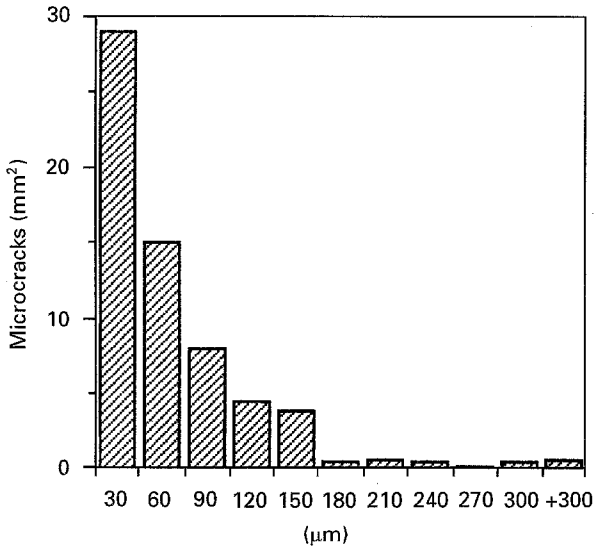

Figure 19 Histogram showing the secondary microcrack distribution in the treated material with an explosive thickness of 1.5 mm for a plastic strain amplitude $\Delta\varepsilon_p/2 = 10^{-3}$, and a total density of 62 mm^{-2}.

specimens are only a third of those of the unpolished specimen. However, on the specimen polished for 75 μm, the microcrack density in the second and third classes is higher than that observed on the specimen polished for 40 μm or on the unpolished specimen. These facts can easily be correlated, on the one hand, with the surface roughness which is better on the treated and polished specimens (R_a close to 0.01 μm instead of 0.45 μm), and on the other hand, with the residual stresses which act on the short cracks (length less than 120 μm on the surface, i.e. depth less than 50–60 μm because the ratio between the depth of a crack and its visible length on the surface is close to 0.4–0.5 [21]). In the case where the residual stresses are in compression at the surface (specimen polished for 40 μm), the microcracks in the first classes are less numerous than those on the unpolished specimen. The compressive residual stresses delay the microcrack initiation and slow down their propagation through the whole compression depth (40–50 μm) which corresponds to microcracks of about 100 μm in length at the surface. On the other hand, if the polishing brings to the surface an area with very low compressive residual stresses (polishing for 75 μm), the microcracks quickly reach an area free of compressive residual stresses, and their initiation and propagation become easier; the microcracks in the second and third classes are thus more numerous than after polishing for 40 μm (Fig. 19).

It thus appears that the effect of the treatment on the fatigue life results in a competition between detrimental effects, such as a ductility decrease of the surface layers, twinning, residual stresses in tension in the external layer, the increase of cyclic stress or of plastic strain amplitude in the bulk, and beneficial effects such as the decrease of the plastic strain amplitude in the surface layers, compressive residual stresses under the surface layer. Owing to the mode of deformation with an applied plastic strain, the resulting effect is negative. So, in order to obtain beneficial effects on the fatigue life, it would be necessary to realize tests in a stress-controlled mode. Such tests will be performed and results published later.

5. Conclusion

A type 316L stainless steel was treated by a primary explosive with thickness in the range 0.5–1.5 mm, then tested in fatigue with a constant plastic strain amplitude in the range 10^{-3} to 5×10^{-3}.

The treatment induces in the material a marked hardening, especially in the first 300 μm. The surface roughness factor after treatment remains low. The microstructure is mainly characterized by a profuse twinning in the highly strengthened layers. The residual stresses at the surface are in tension. Beneath 10 μm depth, they are in compression up to about 100 μm.

The cyclic behaviour of the treated samples is characterized by a higher stress amplitude than for the untreated material during the near totality of the test. This behaviour is explained by the very high strengthening induced by the treatment. However, the fatigue life of the treated material is shorter than the reference one. On the other hand, the secondary microcrack density of the treated material is much higher than that of the untreated material, especially for the very short cracks. The characterization of the induced effects and the use of tests performed on treated then polished samples, allow both the shorter fatigue life and the higher microcrack density to be explained. They are due to the superposition of detrimental effects on the one hand, such as surface roughness, tension residual stresses in the external layer, twinning, decrease of ductility of the surface layers, increase of cyclic stress and plastic strain amplitude in the bulk, and on the other hand, beneficial effects such as decrease of the plastic strain amplitude in the surface layers and compressive residual stresses beneath the surface layer.

Acknowledgement

The authors thank Professor K. F. Badawi for his help in preparing the residual stress measurement technique.

References

1. H. WOHLFARHT, in "Proceedings of the 2nd International Conference on Shot Peening, Chicago, May 1984, pp. 316–31.
2. B. GENTIL, M. DESVIGNES and L. CASTEX, *Materiaux Techniques*. December (1987) 493.
3. P. BALLARD, Thesis, Ecole Polytechnique, Palaiseau (1991).
4. J. FOURNIER, *J. Phys. III* **1** (1991) 1467.
5. P. PEYRE, Thesis, Compiègne (1993).
6. H. P. LIEURADE and J. F. FLAVENOT, "Fatigue et traitements de surface", Journées de Printemps de la SFM (1987) pp. 1–42.
7. C. DUBOUCHET, Thesis, Orsay (1993).
8. J. P. DUFOUR, Thesis, Poitiers (1990).
9. M. GERLAND, J. P. DUFOUR, H. N. PRESLES, P. VIOLAN and J. MENDEZ, *J. Phys. III* **1** (1991) 1647.
10. M. GERLAND, H. N. PRESLES, J. MENDEZ and J. P. DUFOUR, *J. Mater. Sci.* **28** (1993) 1551.

11. M. GERLAND, M. HALLOUIN and H. N. PRESLES, *Mater. Sci. Eng.* **A156** (1992) 175.
12. L. PAILLE, M. GERLAND, J. P. VILLAIN, K. F. BADAWI, H. N. PRESLES and B. BOUCHET, *J. Phys. III* **4** (1994) 305.
13. L. PAILLE, M. GERLAND and H. N. PRESLES, *DYMAT J.* **1** (2) (1994) 109.
14. L. PAILLE, Thesis, Poitiers (1994).
15. M. GERLAND and L. FOUILLAND-PAILLE, to be published.
16. C. BELAMRI, Thesis, Poitiers (1986).
17. P. VIOLAN, J. MENDEZ, C. BELAMRI, C. GORLIER, J. H. DRIVER and C. AMZALLAG, Journées de Printemps de la SFM (Societé Francaise de Metallurgic, 1986) pp. 219–31.
18. J. MENDEZ, M. GHAMMOURI and P. VIOLAN, in "Strength of Metals and Alloys", Vol. 1, ICSMA 8, edited by P. O. Kettunen, T. K. Lepistö, M. E. Lehtonen (Pergamon Press, Oxford, 1988) pp. 849–54.
19. J. MENDEZ and P. VIOLAN, in "Processus d'Endommagement et Cumul des Dommages en Fatigue", Journées de Printemps de la SF2M, Ed. Rev. Metall. **5** (1991) pp. 58–63.
20. G. CHALANT and L. REMY, *Acta Metall.* **28** (1980) 75.
21. R. ROUX, Thesis, Poitiers (1986).

Received 21 March
and accepted 17 October 1995